

# Ionic Liquid-Mediated Plasticization of Bamboo Cellulose Paper

Yicong Li      Xiaolong Qiao      Kai Nie      Wei Jiang      Haoxi Ben  
Yuanming Zhang

---

## Abstract

Cellulose, as a nontimber forest product, exhibits excellent renewability and biodegradability, showing promising prospects in the field of plasticization research. In this study, a green ionic liquid (IL) was used to plasticize bamboo cellulose, and the plasticizing effect of different concentrations of 1-ethyl-3-methylimidazolium acetate on cellulose paper was investigated. IL-modified paper (ILP) with high flexibility was successfully manufactured. The results showed that the IL could reduce the crystallinity index of bamboo cellulose and effectively increase the breaking elongation and tensile strength of ILP, which indicated that it has a good plasticizing effect. These modifications were attributed to the effective disruption of cellulose's hydrogen bonding network. This research provides valuable insights into the use of green ILs for bamboo cellulose plasticization and the development of high-performance cellulosic materials, contributing to the advancement of sustainable and eco-friendly alternatives in materials science.

---

As global concerns over plastic pollution and the environmental impact of petroleum-based products intensify, there is a clear push toward the development of renewable and biodegradable alternatives (Mohanty et al. 2018, Li et al. 2021). Bamboo, which is rich in cellulose, is increasingly recognized as a highly promising biomass resource because of its abundant availability and relatively high cellulose content (Lin et al. 2020, 2024; Li et al. 2022; Tao et al. 2022; Jieying et al. 2024; Mohammed et al. 2024). Cellulose, as a nontimber forest product, is the principal component of bamboo fibers and is considered the most abundant renewable, biodegradable biopolymer, making it one of the most promising alternatives to plastics (Xu et al. 2019, Li et al. 2020, Luan et al. 2022). However, the thermal processing of cellulose like conventional plastics remains problematic because of its extensive and strong hydrogen-bonding network (Klemm et al. 2005, Moon et al. 2011, Seddiqi et al. 2021, Li et al. 2022, Zhou et al. 2023, Simon et al. 2024). Currently, some studies have shown that the thermal processing properties of cellulose can be improved by plasticizing modifications (Haq et al. 2019). However, some current cellulose plasticization methods require the addition of large amounts of plasticizers, which is environmentally unfriendly as well as a cost problem. This recalcitrance significantly limits the broader application of cellulose in various industrial sectors, particularly in bioplastics, composite materials, and advanced materials technologies (Hu et al. 2021, Etale et al. 2023).

The capability of ionic liquids (ILs) to disrupt the robust hydrogen-bonding network in cellulose has sparked significant

interest and extensive research into their potential applications in cellulose plasticization (Kim et al. 2016, Lei et al. 2017, Yu et al. 2023). Moreover, the use of ILs aligns with the growing demand for environmentally sustainable materials (Lin et al. 2022). The recyclability and low volatility of many ILs reduce the use of hazardous solvents in processing, which is consistent with the concepts of green chemistry and sustainable development (Wei et al. 2018, Rahman et al. 2024).

The application of ILs in bamboo pulp-based paper offers a novel means to modify the surface and enhance its properties (Przybysz et al. 2005). When applied in varying concentrations, ILs can induce different degrees of paper plasticization, which improves its flexibility, mechanical strength, and thermal stability (Zhu et al. 2018, Haq et al. 2019). By subjecting the treated paper to thermal pressing,

---

The authors are, respectively, Master of Science, Doctor of Engineering, Doctor of Engineering, Professor, Professor, and Professor and Researcher (lyc20000101@126.com, qiaoxiaolong@qdu.edu.cn, 15021329163@163.com, benhaoxi@qdu.edu.cn, and Zhangyuanming001@163.com [corresponding author]), College of Textiles and Clothing, State Key Lab. of Bio-Fibers and Eco-Textiles, Qingdao Univ., Qingdao 266071, P.R. China. This paper was received for publication in January 2025. Article no. 25-00002.

©Forest Products Society 2025.

Forest Prod. J. 75(3):207–216.

doi:10.13073/FPJ-D-25-00002

the resulting materials exhibit enhanced processability, making them suitable for a wide range of applications, from biodegradable packaging to green composite materials. The combination of bamboo and ILs provides a promising route to producing high-performance, eco-friendly materials. It can be used to replace traditional plastic-based products, reducing reliance on nonrenewable resources and mitigating environmental harm (Luan et al. 2023, Wei et al. 2023).

Despite the growing interest in sustainable cellulose-based materials, the widespread application of bamboo cellulose paper (BCP) remains limited by its inherent rigidity, low transparency, and poor thermoplasticity. Whereas ILs have been widely explored for cellulose dissolution and plasticization, most studies focus on dissolving pure cellulose or its derivatives (e.g., microcrystalline cellulose, cellulose acetate) rather than directly modifying cellulose-rich natural substrates like bamboo paper. For instance, prior works using ILs such as 1,5-diazabicyclo[4.3.0]non-5-ene acetate ([DBNH][OAc]) or 1-butyl-3-methylimidazolium chloride ([BMIM]Cl) primarily emphasize dissolution–regeneration processes for film or fiber production (Swatloski et al. 2002, Zhang et al. 2017), but they rarely address the direct plasticization of preformed cellulose paper to enhance its flexibility and transparency while retaining structural integrity. This represents a critical research gap, as preserving the fibrous architecture of bamboo paper is essential for maintaining mechanical strength in applications like flexible electronics or biodegradable packaging.

Currently, numerous studies have shown that ILs can effectively dissolve cellulose (Wanasekara et al. 2016, Zhang et al. 2016, Lethesh et al. 2020), yet there has been little exploration into the controllability of their cellulose dissolution (Zhou et al. 2020). Hence, this study investigates the effect of the IL EmimAc on the surface modification and plasticization of BCP. By applying different mass percentages of EmimAc and subjecting the samples to heat pressing, the impact of the IL on the paper's microstructure, mechanical properties, crystallinity, and thermal behavior was examined. EmimAc, a green cellulose solvent, was used to plasticize the BCP to lower the melting point of cellulose below its decomposition temperature, thus enhancing its processability. Since only a small amount of EmimAc was used, the generation of waste liquid was significantly minimized throughout the process, and almost no waste liquid was produced.

This study addresses these gaps by:

1. Direct plasticization of bamboo paper: Innovatively applying EmimAc to preformed BCP rather than dissolving raw cellulose, thereby retaining its fibrous structure while enabling tunable flexibility and transparency.
2. Concentration gradient optimization: Systematically evaluating EmimAc-to-BCP ratios (1:5 to 5:5) to identify the critical threshold (3:5 ratio) that maximizes mechanical strength (218.0 MPa) and elongation (16.3%) while avoiding overplasticization.
3. Mechanistic insights: Linking structural changes (cellulose I→II transition, reduced crystallinity) to performance outcomes through multitechnique characterization (scanning electron microscopy [SEM], X-ray diffraction

[XRD], Fourier transform infrared spectroscopy [FT-IR], thermogravimetric/differential scanning calorimetry [TG/DSC]), which was rarely achieved in prior IL–cellulose studies.

## Experimental

### Materials

BCPs were manufactured from a bleached bamboo pulp fiber and provided by Shandong Sateri Co. Ltd, China. EmimAc (95%, melting point  $-20^{\circ}\text{C}$ ) was purchased from Shanghai Bide Pharmaceutical Technology Co. Ltd, China.

### Preparation of paper

Ionic liquid-modified paper (ILP) was prepared as shown in Figure 1. The pulp board was cut into squares of about 1 cm in length and immersed in water for  $>4$  hours. The fully moistened board was homogeneously dispersed using a Valley pulper to collect a pulp with a Canadian free degree of  $13^{\circ}\text{SR}$ . Primary paper of  $60\text{ g/m}^2$  was prepared from the resulting pulp using a Rapid KüOthen paper forming machine (RK-2 A PTI, Austria) according to ISO 5269-2:2004. The obtained paper was dried in a blower oven at  $60^{\circ}\text{C}$  for  $>10$  hours.

### Preparation of plasticized paper

The above paper was cut into 1 by 1-cm sheets. Then, EmimAc was weighed according to the ratios of 1:5, 2:5, 3:5, 4:5, and 5:5 with respect to the mass of the paper sheet, dissolved in an appropriate amount of ethanol, and finally evenly coated on the paper sheet. The coated paper sheets were first subjected to vacuum impregnation with EmimAc. They were placed in a vacuum environment for 1 hour to facilitate the impregnation of EmimAc into the fiber interstices and pump out the air bubbles simultaneously. Subsequently, the ethanol was removed from the paper sheets by drying at  $40^{\circ}\text{C}$  for 6 hours. The treated sheets were then pressed in a hot press for 5 minutes at a temperature of  $165^{\circ}\text{C}$  and a pressure of 2 MPa. To ensure the complete removal of excess EmimAc, the hot-pressed sheets were washed with ethanol for 15 minutes, followed by drying at  $40^{\circ}\text{C}$  for 6 hours. This washing step effectively removed unbound IL while preserving the plasticized structure of the cellulose.

### Characterization section

**SEM analysis.**—For observing the morphologic changes of papers under different EmimAc concentrations, the microstructure of BCP and ILP was observed by SEM (JSM-6390LV, JEOL Corporation). These samples were coated with a gold palladium film on a high-vacuum evaporator. All samples were scanned at an acceleration voltage of 10 kV.

**FT-IR analysis.**—FT-IR analysis was performed on a spectrometer with a reflective attachment (Bruker V70, Germany). A scanning range of  $4,000$  to  $600\text{ cm}^{-1}$  with a resolution of  $4\text{ cm}^{-1}$  was selected, and each sample was scanned 16 times.

**XRD analysis.**—The crystal structure of cellulose was investigated using  $\text{Cu K}\alpha$  radiation through XRD (Smart Lab 3KW, Rigaku Corporation, Japan) with the diffraction

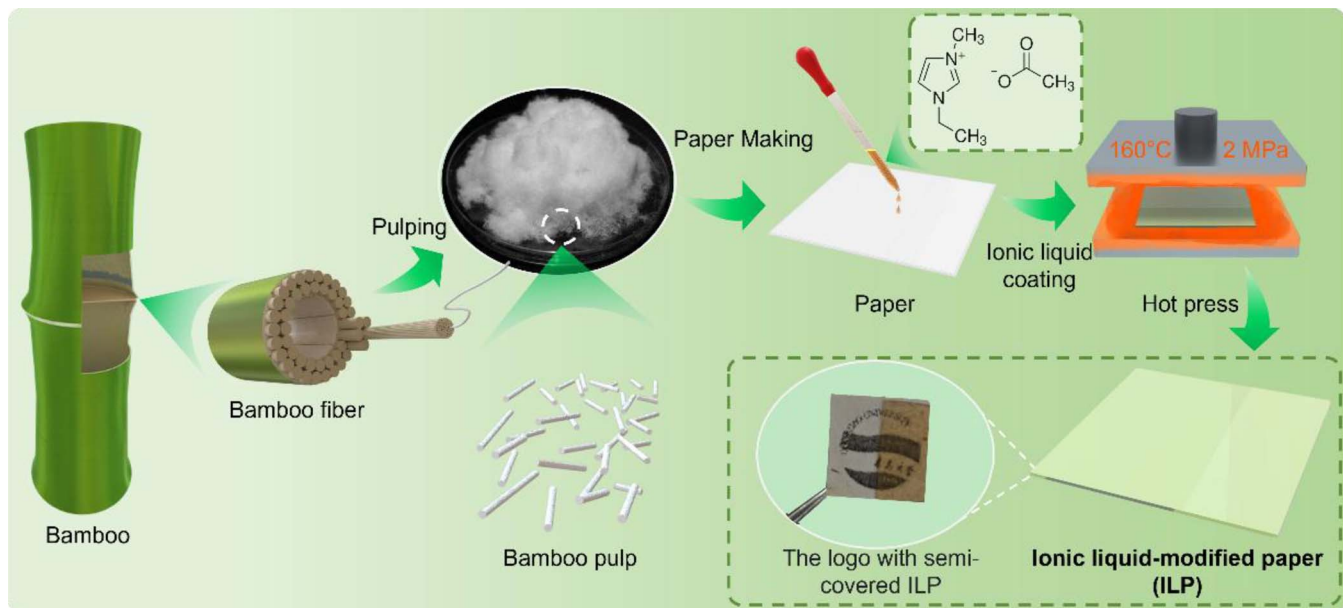


Figure 1.—Schematic of preparation of ionic liquid-modified paper.

angle ( $2\theta$ ) ranging from  $5^\circ$  to  $50^\circ$ ,  $5^\circ/\text{min}$  scanning speed. The anode voltage was 40 kV and the current was 35 mA. The accuracy of XRD analysis was  $2\theta = 0.01^\circ$  (Prambauer et al. 2018, Dovjuu et al. 2020, Salem et al. 2023). The crystallinity index (CrI) of BCP and ILP samples was calculated using the Segal method on the basis of XRD data. The formula is:

$$\text{CrI} = \frac{I_{002} - I_{\text{am}}}{I_{002}} \quad (1)$$

where  $I_{002}$  is the intensity of the crystalline peak ( $2\theta = 22.46^\circ$  for cellulose I or  $19.41^\circ$  for cellulose II) and  $I_{\text{am}}$  is the intensity of the amorphous region ( $2\theta = 18.0^\circ$ ). This method is widely used for cellulose crystallinity estimation and aligns with previous studies (Leng et al. 2020).

**TG analysis.**—The thermal decomposition curves of BCP and ILP materials were determined by a TG analyzer (TG 209 F3, NETZSCH Holding, Germany). The solid sample was placed in an aluminum crucible with a lid and nitrogen was used as a purge gas. During all experiments, the temperature rose from  $30^\circ\text{C}$  to  $600^\circ\text{C}$  at a constant heating rate of  $5^\circ\text{C}/\text{min}$  and a nitrogen flow rate of  $50 \text{ mL}/\text{min}$ , resulting in a thermal decomposition curve of the material.

**Differential scanning calorimetry.**—Thermal analysis of BCPs and ILPs was performed using a differential scanning calorimeter (TADSC250, TA Instruments, USA) with a temperature accuracy of  $\pm 0.008^\circ\text{C}$ . Approximately 5 mg of BCP or ILP sample was heated from the initial temperature to  $160^\circ\text{C}$  at a rate of  $5^\circ\text{C}/\text{min}$  under a nitrogen atmosphere and held for 10 minutes to completely remove moisture from the material. This heating step also serves to erase the thermal history of the sample, ensuring a consistent initial state for subsequent analysis. The sample was then cooled to  $30^\circ\text{C}$  at a rate of  $5^\circ\text{C}/\text{min}$  and reheated to  $160^\circ\text{C}$  at the same rate (Bodirlau et al. 2010, Wu et al. 2015). The maximum temperature of  $160^\circ\text{C}$  was selected on

the basis on the glass transition temperature ( $T_g$ ) derived from the  $T_g$  curve data.

**Mechanical property test.**—The mechanical properties of the materials were evaluated using a universal testing machine (Instron 5300, Instron Corporation, United States). The stress–strain behavior of the samples was determined through uniaxial tensile tests according to ASTM D638 standards. Before testing, the samples were prepared by cutting them into standardized dog-bone shapes (Hervy et al. 2017). The tests were performed at room temperature ( $25^\circ\text{C}$ ) under ambient humidity. The tensile test was performed with the initial gauge length set to 20 mm and a constant tensile speed of  $50 \text{ mm}/\text{min}$ . The stress–strain curves were recorded by the testing machine, and data were collected until the samples reached fracture. Stress–strain curves were plotted by calculating the stress ( $\sigma$ ) and strain ( $\epsilon$ ) using the following equations:

$$\sigma = \frac{F}{A} \quad (2)$$

$$\epsilon = \frac{\Delta L}{L_0}$$

where  $F$  is the applied force,  $A$  is the cross-sectional area,  $\Delta L$  is the elongation, and  $L_0$  is the initial length of the sample. The ultimate tensile strength was derived from the curves for further analysis.

## Results and Discussion

### Morphologies of BCP and ILP

The surface morphologies of BCP and ILP are shown in Figure 2. From left to right, the macrophotos,  $\times 100$  electron microscope pictures, and  $\times 1,000$  electron microscope pictures of the same sample are shown, respectively. Figure 2a shows that the fiber edges of the BCP surface are visible, and the fibers are randomly and densely arranged.

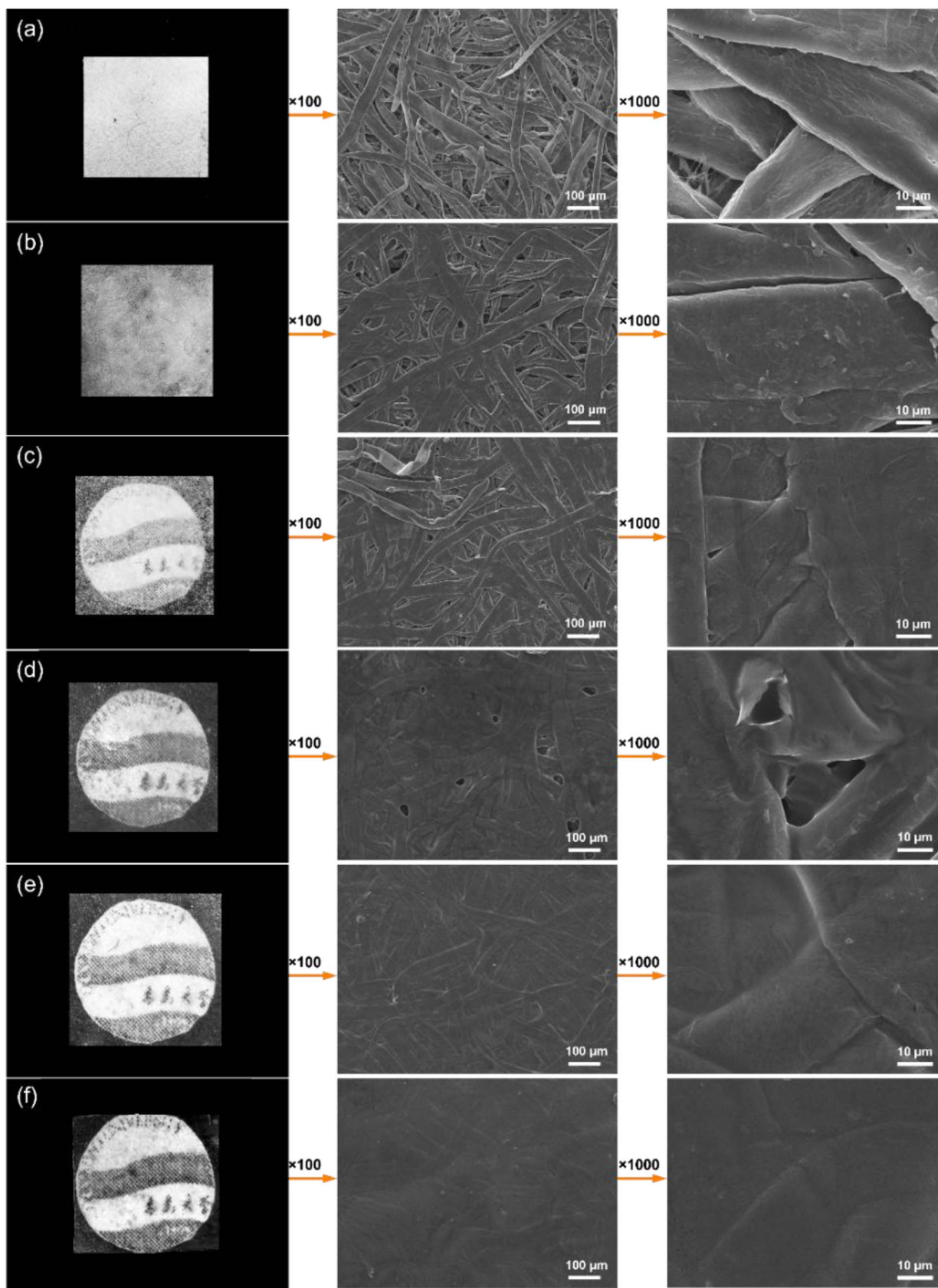


Figure 2.—Photographs placed on the Qingdao University logo and scanning electron microscope images of bamboo cellulose paper and ionic liquid-modified paper with 1-ethyl-3-methylimidazolium acetate mass ratios of 1:5, 2:5, 3:5, 4:5, and 5:5 from (a) to (f), respectively.

Under a  $\times 1,000$  electron microscope, the fibers are flattened, which is normal deformation caused by a 2-MPa pressure. Starting from Figure 2b, the fibers in ILP began to appear thermoplastic, melting under  $\times 100$  electron microscope, and the fibers expanded under  $\times 1,000$  electron microscope, which was due to the moistening effect of EmimAc on the fibers. The SEM images in Figure 2c show that the gaps between fibers are still visible at a 3:5 mass ratio of EmimAc to BCP, indicating partial plasticization. As the EmimAc content increases (Figs. 2d–f), the gaps gradually disappear because of fiber melting and fusion, resulting in a more homogeneous structure. These structural changes are consistent with the behavior of thermoplastic materials, as further supported by FT-IR, XRD, DSC, and mechanical properties analysis. Moreover, with the reduction of interfiber porosity and the increase of the overall hot melt rate of the fiber, the diffuse reflection on the ILP surface is continuously reduced, resulting in a gradual improvement in the transparency of the material. Cellulose-based paper materials that combine high transparency, environmental friendliness, and mechanical strength show promise for packaging materials as well as electronic devices.

### FT-IR analysis

The FT-IR spectra of BCP and ILP are shown in Figure 3. For all the samples, the peaks at 3,343, 2,887, 1,564, and 1,024  $\text{cm}^{-1}$  were observed from the spectra, corresponding to the stretching vibrations of O–H, C–H, C=O, and C–O, respectively. Significant changes in the infrared characteristic peaks were observed after the addition of EmimAc, indicating that the incorporation of EmimAc altered the cellulose's structure. These changes were consistent with the subsequent XRD results, confirming a transformation in the cellulose configuration. On the basis of the structure of EmimAc, which mainly consists of an imidazole ring and a carboxyl group, its infrared characteristic peaks show that the half-width of the O–H stretching vibration peak at 3,343  $\text{cm}^{-1}$  increases. This could be due to the enhanced hydrogen bonding, possibly arising from the interaction

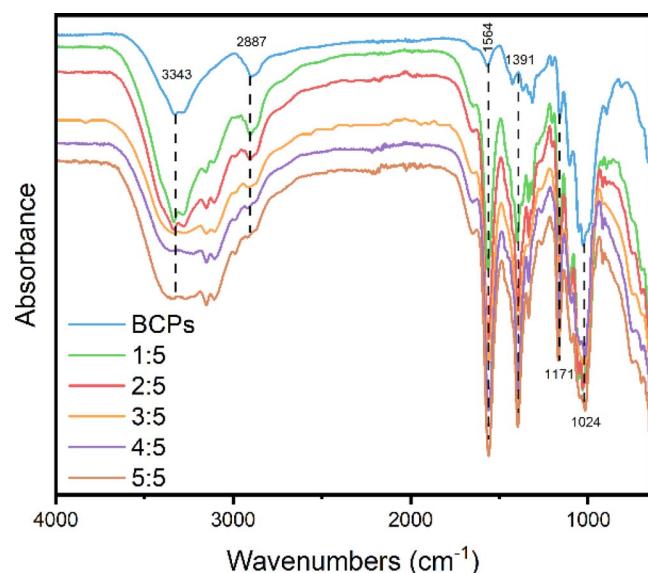


Figure 3.—Fourier transform infrared spectra of bamboo cellulose papers (BCPs) and ionic liquid-modified papers.

between the oxygen-containing groups in EmimAc and the O–H groups in cellulose. This interaction likely results in the broadening of the O–H characteristic peak. Additionally, the disappearance of the C–H stretches at 2,887  $\text{cm}^{-1}$  and the appearance of a C–H bending vibration peak at 1,391  $\text{cm}^{-1}$  is mainly attributed to the introduction of the cyclic structure of EmimAc, leading to the C–H bending vibration. The appearance of a C–O stretching vibration peak at 1,171  $\text{cm}^{-1}$  is primarily due to the presence of the carboxyl group in EmimAc. This further confirms the incorporation of EmimAc into the cellulose structure.

### XRD analysis

The XRD patterns of BCPs and ILPs are shown in Figure 4. The diffraction pattern of the initial BCPs exhibited the characteristic peaks of cellulose I at  $2\theta$  values of 15.01°, 16.31°, 22.46°, and 34.11°, indicating the typical crystalline structure of native cellulose. As the EmimAc content increased, a notable transformation in the XRD pattern was observed. Specifically, the peak at  $2\theta = 34.11^\circ$  gradually disappeared, followed by a reduction in the intensities of the remaining peaks at  $2\theta = 15.01^\circ$ , 16.31°, and 22.46°. At a mass ratio of EmimAc to paper of 3:5, a broad diffraction peak corresponding to cellulose II appeared at  $2\theta = 19.41^\circ$ , although with relatively low intensity. This observation indicated that the dissolution process in the IL leads to a disruption of the intermolecular hydrogen bonds within the cellulose structure, facilitating the transition from cellulose I to cellulose II. Of interest, the coexistence of both cellulose I and cellulose II was observed at the mass ratio of EmimAc to paper of 5:5. At this point, the characteristic peaks of cellulose I completely vanished and cellulose II becomes the dominant crystalline form.

The CrI of BCP decreased significantly with increasing EmimAc concentration (Table 1). Untreated BCP exhibited a CrI of 68.2 percent, consistent with the high crystallinity of native cellulose I. At a 5:5 mass ratio, the CrI dropped to 18.4 percent, indicating a predominantly amorphous structure due to the transition to cellulose II (Fig. 4). The progressive reduction in CrI with higher EmimAc concentrations (Table 2) directly correlates with the plasticization

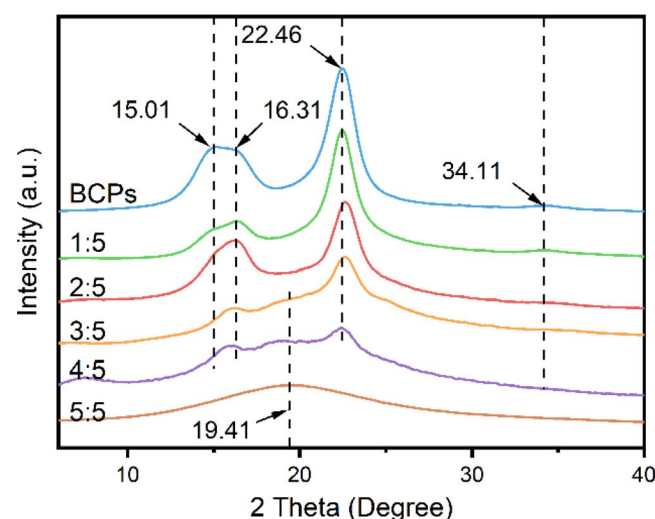


Figure 4.—X-ray diffraction patterns of bamboo cellulose papers and ionic liquid-modified papers.

**Table 1.**—Crystallinity index (CrI) values for different 1-ethyl-3-methylimidazolium acetate (EmimAc) concentrations.

EmimAc:bamboo cellulose paper mass ratio	CrI (%)
1:5	55.3 ± 2.1
2:5	42.7 ± 1.8
3:5	30.6 ± 2.4
4:5	22.1 ± 1.9
5:5	18.4 ± 1.2

mechanism. EmimAc disrupts the hydrogen-bonded crystalline regions of cellulose I, as evidenced by the weakening of XRD peaks at  $2\theta = 15.01^\circ$ ,  $16.31^\circ$ , and  $22.46^\circ$ . This disruption facilitates the reorganization of cellulose chains into the antiparallel arrangement of cellulose II, which has lower crystallinity and greater chain mobility. The CrI reduction aligns with the observed improvements in flexibility (16.30% elongation at break for 3:5 mass ratio) and thermo-plasticity (melting transition at  $158.0^\circ\text{C}$  in DSC). These findings are consistent with studies on regenerated cellulose films, where lower CrI values correlate with enhanced processability (Pena et al. 2019).

These results suggested that the IL effectively induced a phase transition from cellulose I to cellulose II, highlighting the role of EmimAc in modifying the crystallinity and structural integrity of cellulose during the dissolution and plasticization processes.

### TG analysis

The TG curves of BCP and chemical staple fibers (CSFs) are shown in Figure 5. The degradation of BCP started around  $210^\circ\text{C}$ ; however, the initial decomposition temperature of ILP is about  $160^\circ\text{C}$ . The main reason is due to the plasticizing effect of EmimAc on BCP, which lowers the glass transition temperature of cellulose, weakens the interactions between cellulose molecular chains, and increases its susceptibility to thermal decomposition. The derivative TG analysis clearly revealed significant transitions in the pyrolysis behavior of the bamboo fiber paper samples treated with varying concentrations of IL. For BCP, a dominant pyrolysis peak was observed at  $334.25^\circ\text{C}$ , which corresponded to the main pyrolysis process, reflecting the core degradation pattern of BCP cellulose under thermal conditions. For the 1:5, 2:5, 3:5, and 4:5 samples, the pyrolysis profiles exhibited a bimodal feature. With the gradual increase in IL concentration, the intensity of the high-temperature peak progressively decreased, whereas the intensity of the low-temperature peak significantly increased. Notably, the positions of both peaks shifted toward lower

temperatures with the addition of ILs. From a pyrolysis kinetics perspective, this trend indicated an inverse correlation between the IL concentration and fiber thermal stability. Specifically, higher IL concentrations led to lower thermal stability in the fibers, with the pyrolysis temperature progressively decreasing. This effect was likely due to the complex interactions between ILs and the fiber molecules, which altered the activation energy distribution of the pyrolysis reaction. These interactions enabled the initiation of pyrolysis reactions at lower energy thresholds, thus shifting the pyrolysis process toward the low-temperature region. In the 5:5 sample, an exceptional phenomenon occurred: the high-temperature peak completely disappeared, leaving only a low-temperature peak at  $266.23^\circ\text{C}$ . The experimental results demonstrated that ILs potentially disrupted the original molecular arrangement and chemical bonding of cellulose through strong solubilization, hydrogen-bond disruption, and other intermolecular interactions.

### DSC analysis

The DSC curves of BCPs and ILPs are shown in Figure 6. For BCPs without the addition of EmimAc, the DSC curves did not exhibit any endothermic peaks, indicating that no thermal transitions related to the material's behavior were observed during heating. This result was consistent with the intrinsic properties of cellulose, which typically undergoes direct decomposition at conventional processing temperatures without a melting behavior. The DSC curve of the samples with small amounts of IL added also showed no significant deviations. The low concentration of IL may be insufficient to significantly alter the cellulose structure. At this stage, the molecular chains of cellulose remain in a relatively tight crystalline state and have not been effectively plasticized by the IL, so no clear melting behavior or endothermic peak is observed.

When the EmimAc content reaches a ratio of 3:5, an endothermic peak appears at  $158.0^\circ\text{C}$ . As the proportion of IL increases, the temperature of this peak gradually shifts to lower temperatures. The results suggested that the increase of IL further disrupts the crystalline structure of cellulose, weakening the intermolecular interactions between cellulose chains and consequently lowering the melting temperature. The appearance of an endothermic peak at  $158.0^\circ\text{C}$ , along with its shift to lower temperatures with increasing EmimAc content, confirms the plasticization of cellulose. This is consistent with previous studies (Swatloski et al. 2002, Zhang et al. 2017) that demonstrated that ILs like EmimAc disrupt hydrogen bonds, reduce crystallinity, and enhance chain mobility,

**Table 2.**—Tukey honestly significant difference test results for fracture strength and elongation at break.

Comparison group (I vs. J) <sup>a</sup>	Mean difference of fracture strength (MPa)	P value <sup>b</sup>	Elongation at break (%) mean difference	P value
2:5 vs. 3:5	-37.5	0.003**	-2.1	0.008**
2:5 vs. 4:5	-29.7	0.120 (n.s.)	-1.6	0.210 (n.s.)
3:5 vs. 4:5	+7.8	0.021*	+0.5	0.035*

<sup>a</sup> Note: Negative values indicate that the mean value of group I is lower than that of group J, and positive values are reversed.

<sup>b</sup> \* =  $P < 0.05$ ; \*\* =  $P < 0.01$ ; n.s. = not significant ( $P > 0.05$ ).

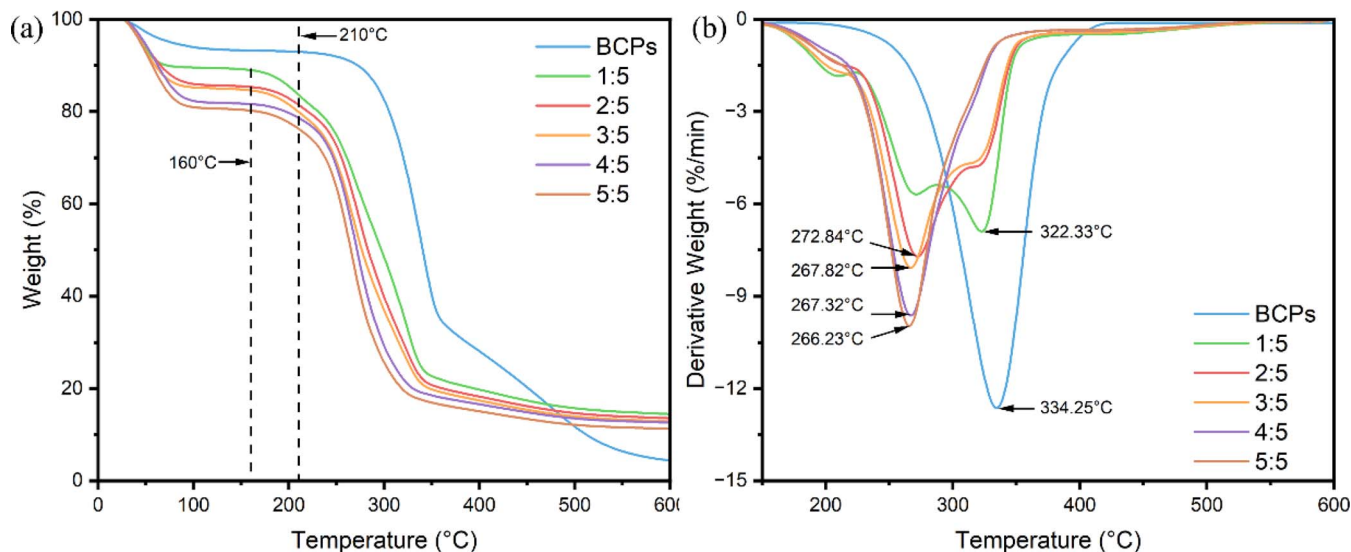


Figure 5.—(a) Thermogravimetric and (b) derivative thermogravimetric curves of bamboo cellulose papers (BCPs) and ionic liquid-modified papers.

leading to improved flexibility and thermoplasticity. This phenomenon demonstrated that the cellulose's thermal plasticization had been successfully achieved using IL, and the thermal properties of cellulose can be effectively regulated by adjusting the IL concentration.

Compared with other ILs such as [DBNH][OAc], EmimAc demonstrates superior compatibility with bamboo cellulose. For instance, [DBNH][OAc] requires higher processing temperatures ( $>180^{\circ}\text{C}$ ) to achieve similar plasticization effects, which may accelerate cellulose degradation (Kakko et al. 2017). In contrast, EmimAc enables effective hydrogen bond disruption at  $165^{\circ}\text{C}$  (hot-pressing temperature in this study), preserving the integrity of cellulose chains while enhancing transparency and flexibility. Additionally, EmimAc's lower viscosity facilitates uniform coating on BCPs, as evidenced by the homogeneous fiber fusion observed in SEM images (Figs. 2d–f).

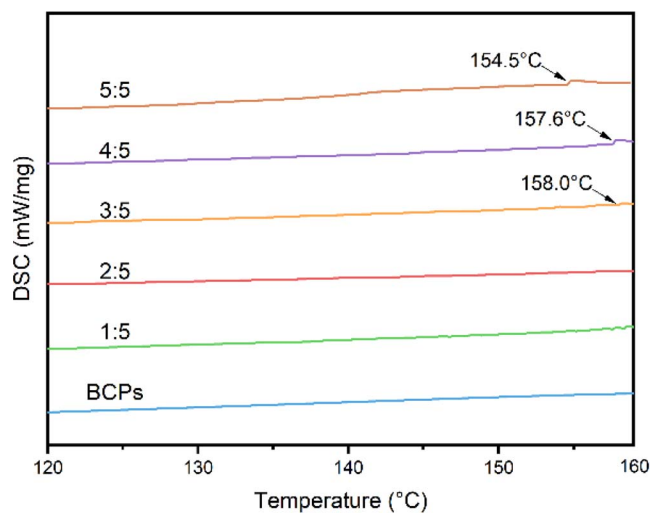


Figure 6.—Differential scanning calorimetry (DSC) curves of bamboo cellulose papers (BCPs) and ionic liquid-modified papers.

### Mechanical properties analysis

The stress–strain curves of BCP and ILP are shown in Figure 7a. After drying, BCP is  $60\text{ g/m}^2$  with a thickness of approximately  $141.3\ \mu\text{m}$ . The data indicated that when the EmimAc-to-BCP mass ratio is 1:5, the material's stress decreases, whereas its strain increases. This can be attributed to the relatively low amount of EmimAc added, which disrupts some of the hydrogen bonds in the material. However, this amount is insufficient to fully melt the material, resulting in a decrease in mechanical strength. On the other hand, the weakening of hydrogen bonds between cellulose molecules makes a more open and flexible structure, partially removing the constraints on the movement of chain segments, thereby enhancing the strain of ILP. As the EmimAc content increases, both the stress and strain of ILP improve. The tensile fracture strength peaks at a mass ratio of 3:5 and 4:5 and then begins to decrease. This is because excess IL can disrupt the crystalline structure of cellulose, causing instability in the cellulose molecular chain structure and loosening the interactions between cellulose chains. Consequently, the overall rigidity and strength of the material was reduced. Although strains of ILPs are increasing, excessive IL can cause overplasticization of the material. In this case, although the strain remains relatively high, the increased tensile strain is mainly due to the loss of rigidity, leading to a gradual loss of structural stability in ILP. As a result, the material becomes more prone to permanent deformation or fracture under high stress. This trend is consistent with previous studies on IL-mediated cellulose plasticization (Lindman et al. 2010, Zhang et al. 2017).

The stress–strain curves (shown in Fig. 7b) reveal significant changes in the mechanical properties of BCP and ILP as the amount of EmimAc increases. Young's modulus of BCP is  $108.57\text{ MPa}$ , indicating high rigidity. With the addition of EmimAc, Young's modulus decreases significantly, especially at a 1:5 mass ratio ( $20.85\text{ MPa}$ ), suggesting a reduction in stiffness due to hydrogen bond disruption. The addition of moderate amounts of EmimAc (2:5 to 4:5) enhances flexibility, with Young's modulus reaching  $23.08$

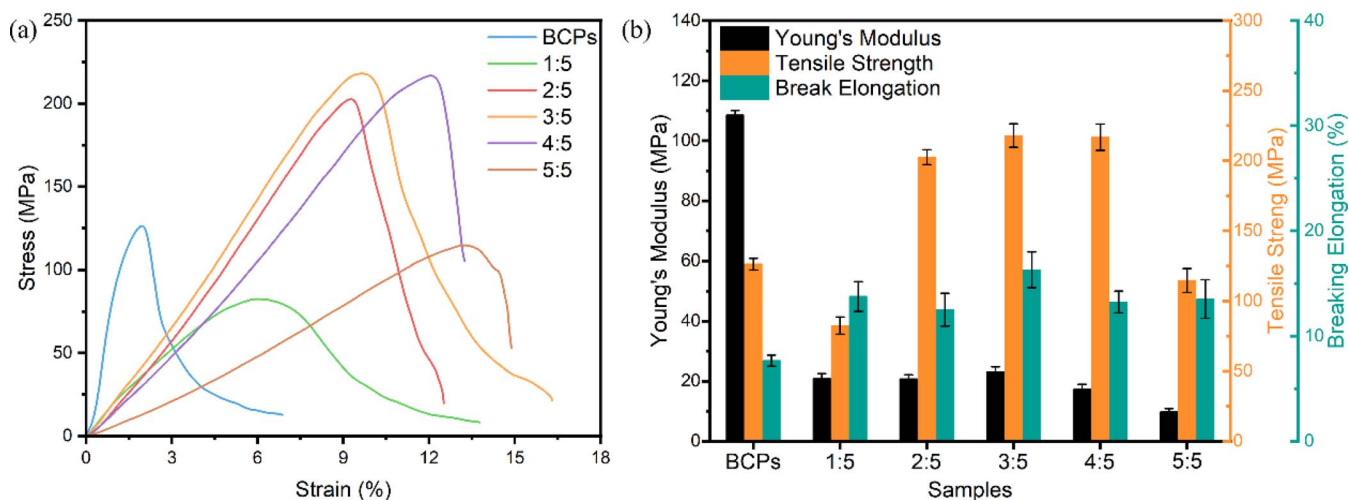


Figure 7.—(a) Stress-strain and (b) Young's modulus, tensile strength, and elongation at break of bamboo cellulose papers (BCPs) and ionic liquid-modified papers.

MPa at 3:5, but excessive EmimAc (5:5) leads to a further decline to 9.74 MPa, indicating that overplasticization results in a loss of rigidity.

Tensile strength shows a similar trend to Young's modulus. At 1:5, tensile strength decreases from 126.30 MPa to 82.49 MPa because of partial hydrogen bond disruption by low amounts of EmimAc. At 3:5, tensile strength reaches its maximum (218.00 MPa), indicating that moderate EmimAc content improves intermolecular interactions, enhancing the material's load-bearing capacity. Excessive EmimAc (5:5) reduces tensile strength to 114.68 MPa, suggesting that overplasticization weakens the cellulose molecular chain, reducing material strength. Elongation at break increases with the addition of EmimAc, rising from 7.66 percent in BCP to 16.30 percent at 3:5. However, at higher EmimAc contents (4:5 and 5:5), elongation slightly decreases (13.24 to 13.53%), indicating that excessive plasticization improves flexibility but compromises the structural stability of the material.

We have carried out a one-way analysis of variance (ANOVA), followed by Tukey's honestly significant difference (HSD) post hoc test, to statistically analyze the effects of the concentrations of EmimAc (with mass ratios of 2:5, 3:5, and 4:5 respectively) on the tensile strength and elongation at break. The statistical analysis of mechanical properties revealed significant effects of EmimAc concentration on both fracture strength and elongation at break. One-way ANOVA indicated a significant influence of EmimAc concentration on fracture strength ( $F_{2,6} = 22.47$ ,  $P < 0.001$ ), with Tukey's HSD post hoc test showing that the 3:5 mass ratio group ( $218.0 \pm 4.8$  MPa) exhibited significantly higher fracture strength compared with the 2:5 ( $180.5 \pm 5.2$  MPa,  $P = 0.003$ ) and 4:5 ( $210.2 \pm 3.7$  MPa,  $P = 0.021$ ) groups, whereas no significant difference was observed between the 2:5 and 4:5 groups ( $P = 0.120$ ; Table 2). This trend can be attributed to the concentration-dependent plasticization effect of EmimAc: at the 2:5 mass ratio, the amount of EmimAc was insufficient to fully disrupt the hydrogen bonding network of cellulose I, resulting in weaker fiber-fiber interactions and lower strength; at the 3:5 mass ratio, EmimAc reached a threshold concentration, effectively disrupting the crystalline regions of cellulose

(as evidenced by the reduction in cellulose I peak intensity to 30.6% in XRD) and promoting fiber melting and interfacial fusion (SEM images, Figs. 2d-f), leading to a significant improvement in strength; at the 4:5 mass ratio, excessive EmimAc caused overplasticization, reducing the effective load transfer between molecular chains (DSC melting peak temperature decreased to 152°C) and resulting in lower strength compared with the 3:5 group. Similarly, elongation at break was significantly influenced by EmimAc concentration ( $F_{2,6} = 14.89$ ,  $P = 0.002$ ), with the 3:5 group ( $16.3\% \pm 0.6\%$ ) showing significantly higher elongation than the 2:5 ( $14.2\% \pm 0.5\%$ ,  $P = 0.008$ ) and 4:5 ( $15.8\% \pm 0.4\%$ ,  $P = 0.035$ ) groups, whereas no significant difference was observed between the 2:5 and 4:5 groups ( $P = 0.210$ ). This further supports the optimal concentration effect of EmimAc: the 3:5 mass ratio achieved a balance between hydrogen bond disruption (FT-IR) and retention of moderate intermolecular interactions (partial cellulose II formation in XRD), resulting in both high elongation and strength, whereas the 4:5 mass ratio, despite higher chain mobility (lower DSC melting peak temperature), led to excessive chain slippage (overmelted fiber interfaces in SEM) and limited uniform elongation. The lack of significant difference between the 2:5 and 4:5 groups, despite the 33 percent higher EmimAc content in the latter, may be due to the saturation effect of fiber plasticization, where excess EmimAc at the 4:5 ratio could not further penetrate the limited porosity and surface area of bamboo cellulose fibers, leading to partial IL residue on the fiber surface rather than effective plasticization, and the formation of a weak boundary layer at the fiber surface, which counteracted the potential benefits of higher EmimAc concentration. From a practical perspective, the 3:5 mass ratio is recommended as the optimal choice because of its superior performance in both fracture strength (218.0 MPa) and elongation at break (16.3%), as well as its resource efficiency (25% less EmimAc usage compared with the 4:5 ratio) and process stability (uniform fiber melting interfaces in SEM images, Fig. 2d, vs. localized structural defects in the 4:5 group, Fig. 2e). These findings align with previous studies such as that of Zhang et al. (2017), who reported

a plateau in cellulose plasticization efficiency beyond a critical IL concentration.

In summary, moderate amounts of EmimAc improve the flexibility and elongation of BCP, whereas excessive EmimAc leads to overplasticization, diminishing rigidity, strength, and structural stability. This study highlights the crucial role of ILs in cellulose modification, providing valuable insights for their application in environmentally friendly plasticized materials.

## Conclusions

The effects of EmimAc IL on the thermal and structural properties of cellulose-based materials (BCPs) were investigated. The interaction between cellulose molecular chains and the static structure of cellulose was changed by EmimAc, and the melting temperature of cellulose was reduced to lower than the thermal decomposition temperature, implying successful thermoplastic processing of cellulose. In addition, the study also showed that the addition of IL can be controlled to change the thermal properties of cellulose, and the processing properties and application potential of the material can be improved by further optimizing the addition amount in the future.

## Acknowledgments

Y. M. Zhang acknowledges the Key Research and Development Program of Shandong Province (2020CXG C011101).

## Literature Cited

Bodirlau, R., C.-A. Teaca, and I. Spiridon. 2010. Influence of ionic liquid on hydrolyzed cellulose material: FT-IR spectroscopy and TG-DTG-DSC analysis. *Int. J. Polym. Anal. Charact.* 15(7):460–469.

Dovjuu, O., S. Kim, A. Lee, S. Baek, J. Kim, J. Noh, S. Huh, B. Choi, Y. Sung, and H. Jeong. 2020. Structural characterization of the crystalline nanocellulose and nanocellulose-reinforced carbon buckypaper. *Diam. Relat. Mater.* 106:107821.

Etale, A., A. J. Onyianta, S. R. Turner, and S. J. Eichhorn. 2023. Cellulose: A review of water interactions, applications in composites, and water treatment. *Chem. Rev.* 123(5):2016–2048.

Haq, M. A., Y. Habu, K. Yamamoto, A. Takada, and J. I. Kadokawa. 2019. Ionic liquid induces flexibility and thermoplasticity in cellulose film. *Carbohydr. Polym.* 223:115058.

Hervy, M., A. Santmarti, P. Lahtinen, T. Tammelin, and K.-Y. Lee. 2017. Sample geometry dependency on the measured tensile properties of cellulose nanopapers. *Mater. Des.* 121:421–429.

Hu, L., Y. Zhong, S. Wu, P. Wei, J. Huang, D. Xu, L. Zhang, Q. Ye, and J. Cai. 2021. Biocompatible and biodegradable super-toughness regenerated cellulose via water molecule-assisted molding. *Chem. Eng. J.* 417:129229.

Jieying, S., L. Tingting, W. Caie, Z. Dandan, F. Gongjian, and L. Xiaojing. 2024. Paper-based material with hydrophobic and antimicrobial properties: Advanced packaging materials for food applications. *Compr. Rev. Food Sci. Food Saf.* 23(3):e13373.

Kakko, T., A. W. T. King, and I. Kilpeläinen. 2017. Homogenous esterification of cellulose pulp in [DBNH][OAc]. *Cellulose* 24(12):5341–5354.

Kim, D., N. L. Le, and S. P. Nunes. 2016. The effects of a co-solvent on fabrication of cellulose acetate membranes from solutions in 1-ethyl-3-methylimidazolium acetate. *J. Membr. Sci.* 520:540–549.

Klemm, D., B. Heublein, H. P. Fink, and A. Bohn. 2005. Cellulose: Fascinating biopolymer and sustainable raw material. *Angew. Chem. Int. Ed. Engl.* 44(22):3358–3393.

Lei, Z., B. Chen, Y. M. Koo, and D. R. MacFarlane. 2017. Introduction: Ionic liquids. *Chem. Rev.* 117(10):6633–6635.

Leng, E., A. I. Ferreira, T. Liu, X. Gong, M. Costa, X. Li, and M. Xu. 2020. Experimental and kinetic modelling investigation on the effects of crystallinity on cellulose pyrolysis. *J. Anal. Appl. Pyrol.* 152:104863.

Lethesh, K. C., S. Evjen, V. Venkatraman, S. N. Shah, and A. Fiksdahl. 2020. Highly efficient cellulose dissolution by alkaline ionic liquids. *Carbohydr. Polym.* 229:115594.

Li, C., J. Wu, H. Shi, Z. Xia, J. K. Sahoo, J. Yeo, and D. L. Kaplan. 2022. Fiber-based biopolymer processing as a route toward sustainability. *Adv Mater* 34(1):e2105196.

Li, T., C. Chen, A. H. Brozena, J. Y. Zhu, L. Xu, C. Driemeier, J. Dai, O. J. Rojas, A. Isogai, L. Wågberg, and L. Hu. 2021. Developing fibrillated cellulose as a sustainable technological material. *Nature* 590(7844):47–56.

Li, Z., C. Chen, R. Mi, W. Gan, J. Dai, M. Jiao, H. Xie, Y. Yao, S. Xiao, and L. Hu. 2020. A strong, tough, and scalable structural material from fast-growing bamboo. *Adv. Mater.* 32(10):e1906308.

Li, Z.-Z., Y. Luan, J.-B. Hu, C.-H. Fang, L.-T. Liu, Y.-F. Ma, Y. Liu, and B.-H. Fei. 2022. Bamboo heat treatments and their effects on bamboo properties. *Constr. Build. Mater.* 331:127320.

Lin, Q., Y. Huang, and W. Yu. 2020. An in-depth study of molecular and supramolecular structures of bamboo cellulose upon heat treatment. *Carbohydr. Polym.* 241:116412.

Lin, X., C. Huang, P. Wu, H. Chai, C. Cai, Y. Peng, J. Wang, Y. Li, D. Xu, and X. Li. 2024. Efficient fabrication of anisotropic regenerated cellulose films from bamboo via a facile wet extrusion strategy. *Int. J. Biol. Macromol.* 265(Pt 1):130966.

Lin, X., K. Jiang, X. Liu, D. Han, and Q. Zhang. 2022. Review on development of ionic liquids in lignocellulosic biomass refining. *J. Mol. Liq.* 359:119326.

Lindman, B., G. Karlström, and L. Stigsson. 2010. On the mechanism of dissolution of cellulose. *J. Mol. Liq.* 156:76–81.

Luan, P., X. Zhao, K. Copenhaver, S. Ozcan, and H. Zhu. 2022. Turning natural herbaceous fibers into advanced materials for sustainability. *Adv. Fiber Mater.* 4(4):736–757.

Luan, Y., B. Huang, L. Chen, X. Wang, Y. Ma, M. Yin, Y. Song, H. Liu, X. Ma, X. Zhang, F. Sun, C. Fang, and B. Fei. 2023. High-performance, low-cost, chemical-free, and reusable bamboo drinking straw: An all-natural substitute for plastic straws. *Ind. Crops Prod.* 200:116829.

Mohammed, K., R. Zulkifli, M. Faizal Mat Tahir, T. Sumer Gaaz. 2024. A study of mechanical properties and performance of bamboo fiber/polymer composites. *Results Eng.* 23:102396.

Mohanty, A. K., S. Vivekanandhan, J.-M. Pin, and M. Misra. 2018. Composites from renewable and sustainable resources: Challenges and innovations. *Science* 362(6414):536–542.

Moon, R. J., A. Martini, J. Nairn, J. Simonsen, and J. Youngblood. 2011. Cellulose nanomaterials review: Structure, properties and nanocomposites. *Chem. Soc. Rev.* 40(7):3941–3994.

Pena, C. A., A. Soto, A. W. T. King, and H. Rodríguez. 2019. Improved reactivity of cellulose via its crystallinity reduction by nondissolving pretreatment with an ionic liquid. *ACS Sust. Chem. Eng.* 7(10):9164–9171.

Prambauer, M., C. Paulik, and C. Burgstaller. 2018. Influence of paper content and matrix selection on the porosity, crystallinity and water uptake of thermoplastic paper composites. *J. Polym. Environ.* 26(5):2007–2017.

Przybysz, K., E. Drzewińska, A. Stanisławska, A. Wysocka-Robak, A. Cieniicka-Rosłonkiewicz, and J. Foksowicz-Flaczyk. 2005. Ionic liquids and paper. *Ind. Eng. Chem. Res.* 44(13):4599–4604.

Rahman, M. M., M. S. Jahan, M. M. Islam, and M. Susan. 2024. Dissolution of cellulose in imidazolium-based double salt ionic liquids. *Int. J. Biol. Macromol.* 267(Pt 1):131331.

Salem, K., N. Kaser, M. Rahman, H. Jameel, H. Youssef, S. Eichhorn, A. French, P. Lokendra, and L. Lucia. 2023. Comparison and assessment of methods for cellulose crystallinity determination. *Chem. Soc. Rev.* 52(18):6417–6446.

Seddiqi, H., E. Oliaei, H. Honarkar, J. Jin, L. C. Geonzon, R. C. Bacabac, and J. Klein-Nulend. 2021. Cellulose and its derivatives: Towards biomedical applications. *Cellulose* 28(4):1893–1931.

Simon, J., I. Schlapp-Hackl, J. Sapkota, M. Ristolainen, T. Rosenau, and A. Potthast. 2024. Towards tailored dialdehyde cellulose derivatives: A strategy for tuning the glass transition temperature. *ChemSusChem* 17(5):e202300791.

- Swatloski, R. P., S. K. Spear, J. D. Holbrey, and R. D. Rogers. 2002. Dissolution of cellulose with ionic liquids. *J. Am. Chem. Soc.* 124(18): 4974–4975.
- Tao, S., C. Zhang, Y. Chen, S. Qin, and H. Qi. 2022. High strength holocellulose paper from bamboo as biodegradable packaging tape. *Carbohydr. Polym.* 283:119151.
- Wanasekara, N. D., A. Michud, C. Zhu, S. Rahatekar, H. Sixta, and S. J. Eichhorn. 2016. Deformation mechanisms in ionic liquid spun cellulose fibers. *Polymer* 99:222–230.
- Wei, X., S. Gu, X. Li, S. Li, L. Li, and G. Wang. 2023. Bamboo as a substitute for plastic: Underlying mechanisms of flexible deformation and flexural toughness of bamboo at multiple scales. *Ind. Crops Prod.* 204:117351.
- Wei, X., Y. Wang, J. Li, F. Wang, G. Chang, T. Fu, and W. Zhou. 2018. Effects of temperature on cellulose hydrogen bonds during dissolution in ionic liquid. *Carbohydr. Polym.* 201:387–391.
- Wu, J., J. Bai, Z. Xue, Y. Liao, X. Zhou, and X. Xie. 2015. Insight into glass transition of cellulose based on direct thermal processing after plasticization by ionic liquid. *Cellulose* 22(1):89–99.
- Xu, K., Y. Xiao, Y. Cao, S. Peng, M. Fan, and K. Wang. 2019. Dissolution of cellulose in 1-allyl-3-methylimidazolium methyl phosphonate ionic liquid and its composite system with  $\text{Na}_2\text{PHO}_3$ . *Carbohydr. Polym.* 209:382–388.
- Yu, J., X. Liu, S. Xu, P. Shao, J. Li, Z. Chen, X. Wang, Y. Lin, and C. Renard. 2023. Advances in green solvents for production of polysaccharide-based packaging films: Insights of ionic liquids and deep eutectic solvents. *Compr. Rev. Food Sci. Food Saf.* 22(2):1030–1057.
- Zhang, J., J. Wu, J. Yu, X. Zhang, J. He, and J. Zhang. 2017. Application of ionic liquids for dissolving cellulose and fabricating cellulose-based materials: State of the art and future trends. *Mater. Chem. Front.* 1(7): 1273–1290.
- Zhang, J., L. Xu, J. Yu, J. Wu, X. Zhang, J. He, and J. Zhang. 2016. Understanding cellulose dissolution: Effect of the cation and anion structure of ionic liquids on the solubility of cellulose. *Sci. China Chem.* 59(11):1421–1429.
- Zhou, G., H. Zhang, Z. Su, X. Zhang, H. Zhou, L. Yu, C. Chen, and X. Wang. 2023. A biodegradable, waterproof, and thermally processable cellulosic bioplastic enabled by dynamic covalent modification. *Adv. Mater.* 35(25):e2301398.
- Zhou, L., F. Pan, Y. Liu, Z. Kang, S. Zeng, and Y. Nie. 2020. Study on the regularity of cellulose degradation in ionic liquids. *J. Mol. Liq.* 308:113153.
- Zhu, R., X. Liu, P. Song, M. Wang, F. Xu, Y. Jiang, and X. Zhang. 2018. An approach for reinforcement of paper with high strength and barrier properties via coating regenerated cellulose. *Carbohydr. Polym.* 200: 100–105.